Energy 212 (2020) 118702

Contents lists available at ScienceDirect

Energy

journal homepage: www.elsevier.com/locate/energy

Analyzing S-Shaped $I-V$ characteristics of solar cells by solving three-diode lumped-parameter equivalent circuit model explicitly

Gongyi Huang, Ying Liang, Xiaofang Sun, Chuanzhong Xu, Fei Yu*

College of Information Science and Engineering, Huaqiao University, Xiamen, 361021, China

ARTICLE INFO

Article history:
Received 20 December 2019
Received in revised form
17 August 2020
Accepted 20 August 2020
Available online 29 August 2020

Keywords:
New generation solar cells
S-shaped $I-V$ characteristics
Lumped-parameter equivalent circuit model
Analytical solution
Current kinks

ABSTRACT

In order to analyze and optimize new generation solar cells' electrostatic performances, lumped-parameter equivalent circuit model is a common method to simulate S-shaped $I-V$ characteristics including linear, exponential, or exponential-like current kinks. Unfortunately, three-diode lumped-parameter model is still inevitable to be solved generally in numerical iteration method. The absence of explicit solution to three-diode lumped-parameter model is actually the main bottleneck of implementing the model into photovoltaic device and circuit simulators in compact. In this paper, to overcome the problem of three-diode model's implementation into simulators, we proposed an explicit solution to the model based on the regional approach, where high accuracy and low computation time cost are the main features of such a solution. Analytical derivation and correction for the solution to transcendent $I-V$ equation in three-diode model leads to high computation accuracy, and avoidance of numerical iteration methods introduces low computation time cost. Finally, numerical iteration results and reconstructed experimental data of solar cells are used to validate the accuracy and applicability of our proposed explicit solution. As a result, high accuracy and efficiency of the explicit solution make it possible to implement three-diode lumped-parameter equivalent circuit model into photovoltaic device and circuit simulators and explain $I-V$ characteristics of new generation solar cells.

1. Introduction

In the recent years, solar energy, as a green source of energy, seems to be a promising clean energy supply. Nowadays, all kinds of solar cells are undergoing the rapid developments and completing large-scale commercialization. In order to satisfy the requirements on realizations of electronics' lightweight and flexible design [1], new generation solar cells, such as perovskite [2–5] and organic [6–9] solar cells, have attracted much attentions and been going through intensive researches, in the industry and laboratory field. In the aspect of power conversion efficiency (PCE), compared with 25% ~ 26% PCE of conventional silicon-based solar cells [10], relative low PCE about 20% ~ 25% imposes restrictions on wide applications of these new generation solar cells. In the aspect of manufacturing process cost including energy consumption and materials' cost, these new generation solar cells are obviously much lower than silicon-based solar cells. In the aspect of working stability and life, perovskite and organic solar cells perform far worse than silicon-based solar cells. In fact, working stability or life is one of the most important challenges which impedes the realization for the industrial applications of perovskite and organic solar cells. Thus, further researches are still needed in the new generation solar cells marked by perovskite and organic solar cells, especially for effects from materials, structures, and processes on $I-V$ characteristics. In fact, $I-V$ characteristics directly demonstrate electrostatic performances of solar cells, including short-circuit current, open-circuit voltage, maximum power, and fill factor. All of these four key parameters have an important impact on PCE of solar cells. Thus, accurate and efficient simulations on $I-V$ curves are necessary for researchers to study the methods of improving solar cells' performances, from the perspective of electrostatic properties. In general, lumped-parameter equivalent circuit models are used to predict $I-V$ curves of solar cells. Unfortunately, the absence of analytical solutions to lumped-parameter equivalent circuit models, in particularly for multiple-diode models, leads to a large consumption of computer resources and restricts models' applications of implementing into photovoltaic device and circuit simulators. Therefore, derivation of explicit solution to multiple-diode models is an important and pressing task to describe S-shaped $I-V$

* Corresponding author.
E-mail address: yufei_jnu@126.com (F. Yu).

https://doi.org/10.1016/j.energy.2020.118702

characteristics with linear, exponential, or exponential-like current kinks of new generation solar cells and overcome the bottleneck of multiple-diode models' implement into photovoltaic device and circuit simulators.

Recently, some reviews [11–13] have been published for modelling solar cells including conventional silicon, perovskite, and organic solar cells. For the conventional silicon-based solar cells, one-diode lumped-parameter equivalent circuit models [14–16] are enough to describe J-shaped I–V characteristics, combining with the corresponding analytical solutions. For the new generation solar cells, one-diode models [14–16] are unable to predict the S-shaped I–V curves. Then, multiple-diode lumped-parameter equivalent circuit models [17–22] are proposed to simulate the S-shaped I–V curves and try to explain the current kink in the first quadrant. F. Araujo de Castro et al. [17] proposed a two-diode lumped-parameter model which can demonstrate the S-shaped I–V curves with linear kinks. Subsequently, F. J. Garcia-Sanchez et al. [18] derived an analytical solution to F. Araujo de Castro's two-diode model [17] and improved it to describe S-shaped I–V curves with exponential kinks by substituting a forward-biased diode for a resistance. In fact, F. J. Garcia-Sanchez's model [18] is a three-diode lumped-parameter model, which is similar as B. Mazhari's model [19]. In some special cases, F. J. Garcia-Sanchez et al. [18,20] derived the analytical solutions to F. J. Garcia-Sanchez's [18] and B. Mazhari's [19] models, respectively. Furthermore, F. Yu et al. [21,22] solved B. Mazhari's model [19] explicitly in any case and improved it to explain the exponential-like kink in the first quadrant. P. J. Roland et al. [23] also suggested a three-diode lumped-parameter equivalent circuit model, as shown in Fig. 1, which gave another step forward in the sequence of the previously proposed lumped-parameter models [17–19] and had an ability of simulating linear, exponential, and exponential-like kinks in the S-shaped I–V curves. Unfortunately, P. J. Roland et al. [23] had to used SPICE to complete the simulations because three exponential items are included in the transcend I–V equation. In fact, it is the absence of analytical solution that limits the implement of P. J. Roland's model [23] into photovoltaic device simulators due to a large amount of computer resource consumption. Therefore, there is still room of improvement left for us to proposed an explicit solution to P. J. Roland's model [23], aiming to accurately and efficiently analyze the S-shaped I–V characteristics with current kinks of new generation solar cells.

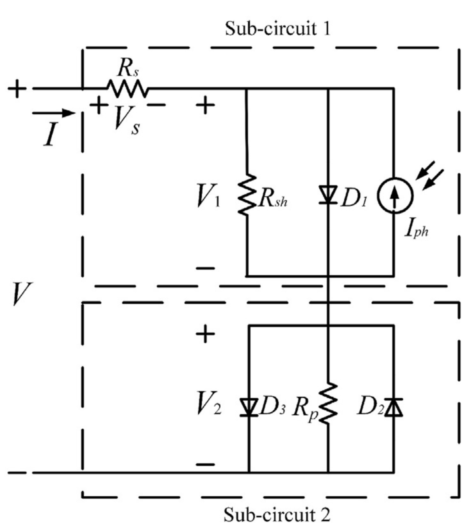

Fig. 1. P. J. Roland's lumped-parameter equivalent circuit model [23], consisting of a conventional one-diode solar cell's lumped-parameter equivalent sub-circuit 1 and a S-shape curve with linear, exponential, or exponential-like kink producing sub-circuit 2.

In this paper, based on the regional approach, the explicit solution to P. J. Roland's lumped-parameter equivalent circuit model is proposed to simulate the S-shaped I–V characteristics with current kinks of new generation solar cells. Firstly, P. J. Roland's model processes wider applications for describing J-shaped I–V curves and S-shaped I–V curves with exponential, linear, or exponential-like kinks. This point is discussed in details from circuit topology and mathematical operation aspects. Subsequently, the regional approach is used to explicitly solve P. J. Roland's lumped-parameter model. Finally, numerical iteration results and reconstructed experimental data measured from perovskite and organic solar cells are adopted to verify the precision and practicability of the proposed explicit solution, respectively. Verification results show that such an explicit solution to P. J. Roland's model can be used to predict both J-shaped and S-shaped I–V characteristics of solar cells accurately and efficiently. As a result, it obviously is convenient to implement P. J. Roland's lumped-parameter equivalent circuit model into photovoltaic device and circuit simulators.

2. Analysis for wide applications of P. J. Roland's lumped-parameter equivalent circuit model

In Fig. 1, P. J. Roland et al. [23] made a crucial improvement from F. Araujo de Castro's [17] and F. J. García-Sánchez's [18] models. Simultaneously, P. J. Roland's model [23] also remains to be compatible with the single-diode lumped-parameter model [24] of the conventional silicon-based solar cells.

According to Fig. 1, the terminal voltage V of equivalent circuit model is expressed as

$$V = V_s + V_1 + V_2. \tag{1}$$

Here, based on Ohm's law, V_s is given by

$$V_s = IR_s; \tag{2}$$

based on Shockley's ideal diode current equation [25], V_1 and V_2 are acquired from the following equations:

$$I = \frac{V_1}{R_{sh}} + I_{01}\left(e^{\frac{V_1}{n_1 V_t}} - 1\right) - I_{ph}, \tag{3}$$

$$I = -I_{02}\left(e^{\frac{-V_2}{n_2 V_t}} - 1\right) + I_{03}\left(e^{\frac{V_2}{n_3 V_t}} - 1\right) + \frac{V_2}{R_p}. \tag{4}$$

For D_1, D_2, and D_3, I_{01}, I_{02}, I_{03} are the reverse saturation currents, n_1, n_2, and n_3 are the ideality factor representing the divergence from the ideal diode. The thermal voltage is symbolized by $V_t = kT/q$, where k is the Boltzmann constant, T is the absolute temperature, and q is the electron charge. In addition, R_{sh} is the shunt resistance representing the leakage current across the PN junction of the conventional solar cells. R_p is a resistance added by P. J. Roland et al. [23] into F. J. García-Sánchez's model [18], and F. J. García-Sánchez's model [18] is modified from F. Araujo de Castro's model [17] by substituting diode D_3 for resistance R_p. In fact, it is R_p that makes P. J. Roland's model [23] process the ability of simulating J-shaped and S-shaped I–V characteristics with current kinks, respectively.

Firstly, in the case of $R_p = 0\ \Omega$, from the circuit topology aspect, sub-circuit 2 in Fig. 1 is shorted, and then P. J. Roland's model [23] could be simplified into one-diode lumped-parameter equivalent circuit model [24] of conventional solar cells, as shown in Fig. 2. From the mathematical operation aspect, considering that the

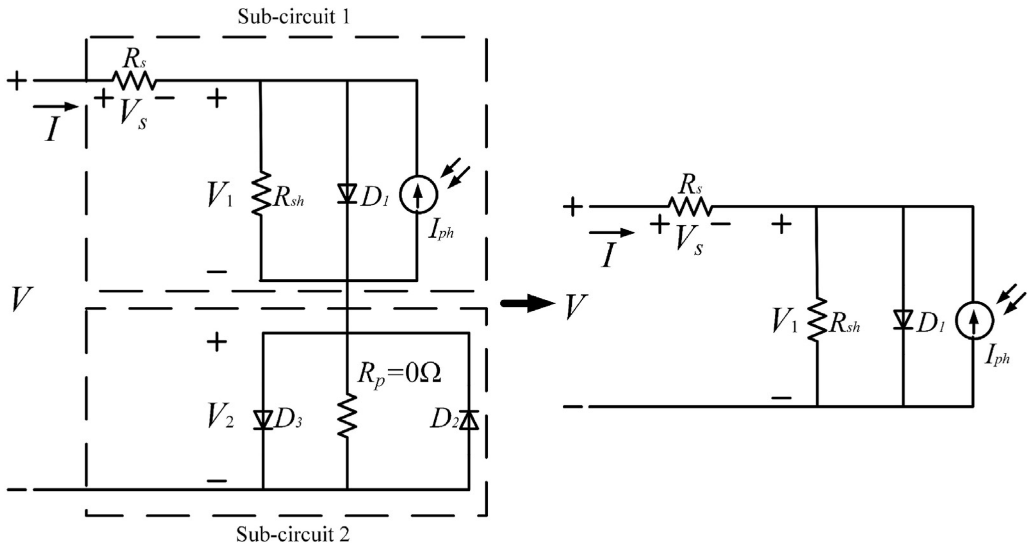

Fig. 2. Transformation from P. J. Roland's model [23] to one-diode lumped-parameter equivalent circuit model [24] of conventional silicon-based solar cells with the ability of explaining the J-shaped I–V curves.

terminal current I could not be infinite, the terminal voltage V_2 of sub-circuit 2 has to be equal to 0 V in (4). From the device physics aspect, the absence of V_2 results in I–V curves' transformation from S-shaped into J-shaped.

Secondly, in the case of $R_p = \infty\ \Omega$, in the view of circuit topology, sub-circuit 2 in Fig. 1 is opened, and subsequently P. J. Roland's model [23] could degenerate into F. J. García-Sánchez's lumped-parameter model [18] of new generation solar cells, as shown in Fig. 3. In the view of mathematical operation, the linear item V_2/R_p in (4) is settled as zero, and then the I–V curves in the first quadrant are determined by D_3 in sub-circuit 2. In the view of device physics, the second exponential item in (4), corresponding with the ideal diode equation of D_3, has the ability of describing S-shaped I–V characteristics with exponential kinks.

Thirdly, in the case of $0\ \Omega < R_p < \infty\ \Omega$, the analysis for P. J. Roland's model [23] could be classified as the following two cases. On the condition that the current going through R_p of the sub-circuit 2 is larger than that going through D_3 in (4), i.e.,

$$I_{03}\left(e^{\frac{V_2}{n_3 V_t}} - 1\right) < \frac{V_2}{R_p} \tag{5}$$

P. J. Roland's model [23] could be equivalent with F. Araujo de Castro's lumped-parameter equivalent circuit model [17], as shown in Fig. 4. From (5), the region of R_p is derived as

$$0\ \Omega < R_p < \left| -\frac{V_2}{I_{03}} - \frac{n_3 V_t}{I_{03}} \cdot W_{-1}\left(-\frac{R_p I_{03}}{n_3 V_t} \cdot e^{-\frac{R_p I_{03}}{n_3 V_t}} \right) \right| \Omega \tag{6}$$

where W_{-1} is the Lambert W function's principal branch [26] as a

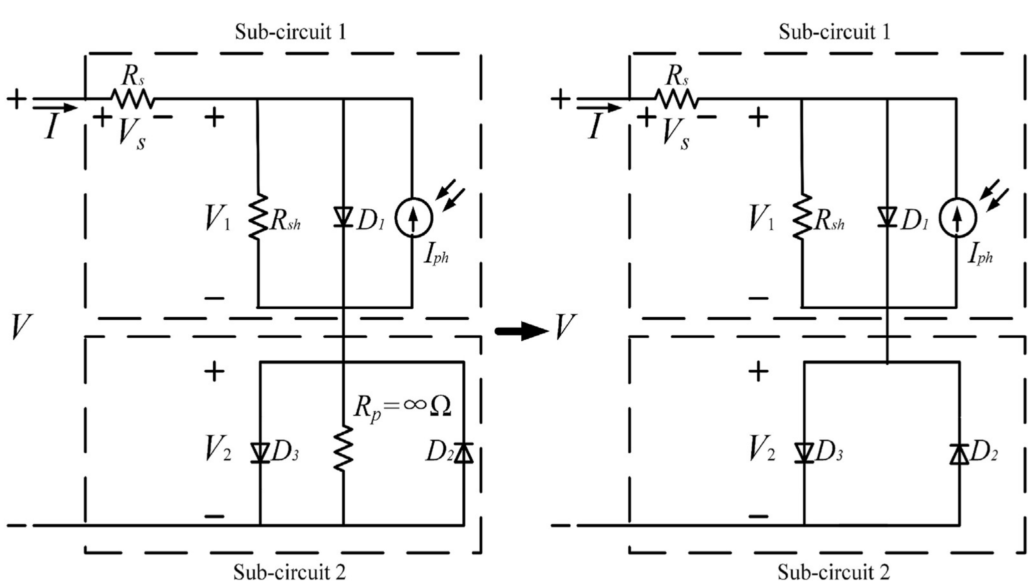

Fig. 3. Transformation from P. J. Roland's model [23] to F. J. García-Sánchez's lumped-parameter equivalent circuit model [18] of new generation solar cells with the ability of explaining the S-shaped I–V curves with exponential kinks.

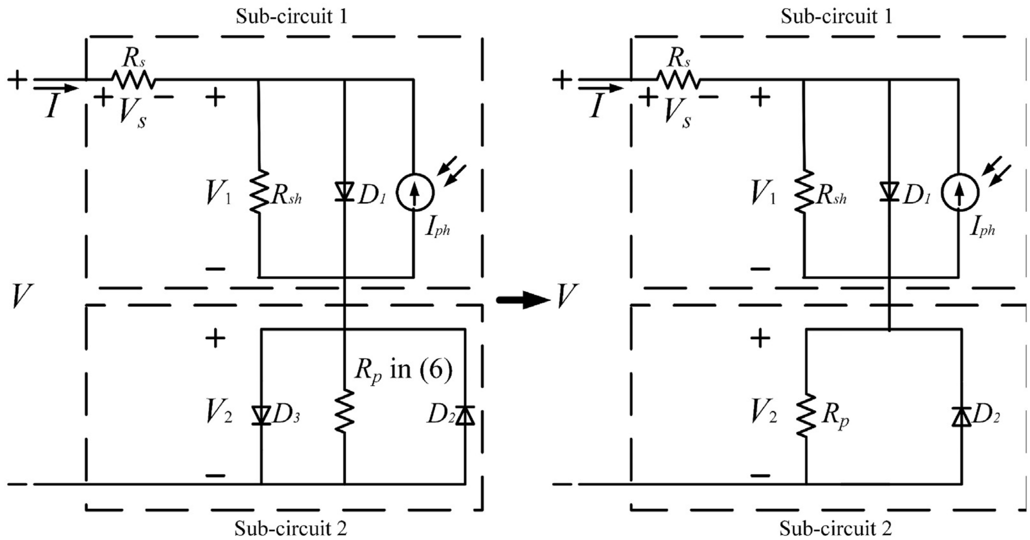

Fig. 4. Transformation from P. J. Roland's model [23] to F. Araujo de Castro's lumped-parameter equivalent circuit model [17] of new generation solar cells with the ability of explaining the S-shaped I–V curves with linear kinks.

typical solution to equation $W_{-1}(x)e^{W_{-1}(x)} = x$ in the case of $x < 0$. In fact, in the case of (6), P. J. Roland's model works similarly as F. Araujo de Castro's model [17] to simulate the S-shaped I–V characteristics with linear kinks. On the condition that the current going through D_3 of the sub-circuit 2 is larger than that going through R_p in (4), i.e.,

$$I_{03}\left(e^{\frac{V_2}{n_3V_t}}-1\right) > \frac{V_2}{R_p} \tag{7}$$

leading to

$$\left| -\frac{V_2}{I_{03}} - \frac{n_3V_t}{I_{03}} \cdot W_{-1}\left(-\frac{R_pI_{03}}{n_3V_t} \cdot e^{-\frac{R_pI_{03}}{n_3V_t}}\right)\right| \, \Omega < R_p < \infty \, \Omega \tag{8}$$

In fact, in the case of (8), P. J. Roland's model [23] performs to simulate the S-shaped I–V characteristics with exponential-like kinks. It is noted that exponential-like kinks are neither exponential nor linear. Of course, in this case, this is both difference and advantage of P. J. Roland's model [23], compared with one-diode model [24], F. J. García-Sánchez's model [18], and F. Araujo de Castro's model [17].

3. Explicit solution to P. J. Roland lumped-parameter equivalent circuit model

According to equation (1) ~ (4), explicitly solving V_1 from (3) and V_2 from (4) is a key to acquire I–V characteristics of solar cells. On the one side, because one exponential item and one linear item of V_1 are observed in the transcend equation (3), V_1 could be analytically solved by using lambert W function's principal branch [26] as a typical solution to equation $W_0(x)e^{W_0(x)} = x$ in the case of $x > 0$, i.e.,

$$V_1 = \left(I_{ph}+I_{01}+I\right)R_{sh} - n_1V_t \times W_0\left[\frac{I_{01}R_{sh}}{n_1V_t} \cdot e^{\frac{\left(I_{ph}+I_{01}+I\right)R_{sh}}{n_1V_t}}\right] \tag{9}$$

In (9), the symbol $W_0[x]$ presents lambert W function's principal branch $x > 0$ where x is represented as $x = \frac{I_{01}R_{sh}}{n_1V_t} \cdot e^{\frac{(I_{ph}+I_{01}+I)R_{sh}}{n_1V_t}}$. On the other side, because two exponential items and one linear item exist in the transcend equation (4), V_2 could not be solved analytically in general. Fortunately, three currents in sub-circuit 2 of Fig. 1 have primary and secondary priorities in the different regions of V_2. Therefore, V_2 could be solved from (4) explicitly by using the regional approach [27,28], which has been widely adopted to build other semiconductor devices' models, such as polysilicon transistors [27], amorphous metal oxide thin-film transistors [28–30], etc.

In the operation region of $V_2 < 0$ V, corresponding to $I < 0$A from (4), the current of D_3 in Fig. 1 could be ignored, i.e., exponential item $I_{03}\left(e^{\frac{V_2}{n_3V_t}}-1\right)$ could be omitted in (4), yielding

$$I = -I_{02}\left(e^{\frac{-V_{2\_sub1}}{n_2V_t}}-1\right) + \frac{V_{2\_sub1}}{R_p} \tag{10}$$

In the operation regime of $V_2 > 0$ V, corresponding to $I > 0$A from (4), the current of D_2 in Fig. 1 could be ignored, i.e., exponential item $-I_{02}\left(e^{\frac{-V_2}{n_2V_t}}-1\right)$ could be neglected in (4), yielding

$$I = I_{03}\left(e^{\frac{V_{2\_sub2}}{n_3V_t}}-1\right) + \frac{V_{2\_sub2}}{R_p} \tag{11}$$

In (10) and (11), $V_{2\text{-}sub1}$ and $V_{2\text{-}sub2}$ are asymptotic solutions to V_2 in two operation regions of $V_2 < 0$ V and $V_2 > 0$ V, respectively. It is noted that the curves of both (10) and (11) go through the point ($V_2 = 0$ V, $I = 0$A). Because only one exponential item is included in (10) and (11), $V_{2\text{-}sub1}$ and $V_{2\text{-}sub2}$ could be solved analytically as

$$V_{2\_sub1} = -R_p(-I+I_{02}) + n_2V_t \cdot W_0\left(\frac{R_pI_{02}}{n_2V_t}\cdot e^{\frac{-R_pI+R_pI_{02}}{n_2V_t}}\right) \tag{12}$$

and

$$V_{2\_sub2} = R_p(I+I_{03}) - n_3V_t \cdot W_0\left(\frac{R_pI_{03}}{n_3V_t}\cdot e^{\frac{R_pI+R_pI_{03}}{n_3V_t}}\right) \tag{13}$$

respectively.

Subsequently, according to (12), (13), and the point ($V_2 = 0$ V, $I = 0$A), the coarse solution V_{2_coarse} of V_2 is expressed by the following piecewise function:

$$V_{2\_coarse} = \begin{cases} -R_p(-I+I_{02}) + n_2V_t \cdot W_0\left(\frac{R_pI_{02}}{n_2V_t}\cdot e^{\frac{-R_pI+R_pI_{02}}{n_2V_t}}\right), I<0\text{A} \\ R_p(I+I_{03}) - n_3V_t \cdot W_0\left(\frac{R_pI_{03}}{n_3V_t}\cdot e^{\frac{R_pI+R_pI_{03}}{n_3V_t}}\right), \quad I \geq 0\text{A} \end{cases} \tag{14}$$

In fact, V_{2_coarse} in (14) is not enough accurate due to the ignorance of minor exponential items for the different operational regions.

In order to improve the precise of solution V_2 to (4), Schroder series w is used to correct the coarse solution V_{2_coarse} of V_2, aiming to acquire the exact solution V_2 to (4), i.e.,

$$V_2 = V_{2\_coarse} + w. \tag{15}$$

Here, Schroder series w is able to make the maximum error of V_2 in (15) much lower than that of V_{2_coarse} in (14), compared with the exact solution V_2 in (4). The correction of Schroder series ω [27,29,31] is symbolled as

$$w = \frac{-y/y'}{1-0.5yy''/y'^2}, \tag{16}$$

$$y = -I_{02}\left(e^{\frac{-V_2}{n_2V_t}}-1\right) + I_{03}\left(e^{\frac{V_2}{n_3V_t}}-1\right) + \frac{V_2}{R_p} - I. \tag{17}$$

$$y' = \frac{I_{02}e^{\frac{-V_2}{n_2V_t}}}{n_2V_t} + \frac{I_{03}e^{\frac{V_2}{n_3V_t}}}{n_3V_t} + \frac{1}{R_p}, \tag{18}$$

$$y'' = -\frac{I_{02}e^{\frac{-V_2}{n_2V_t}}}{(n_2V_t)^2} + \frac{I_{03}e^{\frac{V_2}{n_3V_t}}}{(n_3V_t)^2}. \tag{19}$$

In fact, the method that deriving the starting function and then modifying it with Schroder series has been regarded as a universal fashion [27,29,31]. In addition, the formalism of Schroder series w has been described and explained in Appendix of Ref. [31].

In addition, numerical iteration method is used to verify the accuracy of our proposed analytical solution V_2 to (4), as shown in Fig. 5. In Fig. 5(a), good agreements between analytical solution V_2 in (15) and the results of numerical iteration method are acquired. V_{2_sub1} is only accurate for the region of $V_2 < 0$ V, and V_{2_sub2} is only accurate for the region of $V_2 \geq 0$ V. It is noted that computation time consumed by numerical iteration method is about thirty times more than computation time consumed by our proposed explicit solution V_2 in (15). In Fig. 5 (b) and (c), obviously, error of V_2 (as low as 5×10^{-16} V) is much less than error of V_{2_coarse} (about 0.1 V).

Furthermore, V_s in (2), V_1 in (9), and V_2 in (15) are substituted into (1) to obtain the terminal voltage V in P. J. Roland's lumped-parameter equivalent circuit model of Fig. 1. And then, V consisting of V_s, V_1, and V_2 is shown in Fig. 6 ~8. Because the errors of V_2 are as low as 10^{-16} V scale, the errors of V compared with numerical iteration results are also in the range of 10^{-16} V scale, as shown in Fig. 6 (b) ~ 8 (b). In Fig. 6 (a) and 7 (a), on the condition of $R_s = 0\Omega$, I–V curves show exponential kink for relative large R_p and linear kink for relative small R_p, respectively. As shown in Fig. 6 (a), for relative large R_p, I–V curve of P. J. Roland's model [23] is equivalent to that of F. J. García-Sánchez's model [18]. As shown in Fig. 7 (a), for relative small R_p, I–V curve of P. J. Roland's model [23] is equivalent to that of F. Araujo de Castro's model [17]. In fact, these two points are consistent with the analysis of Part 2. In Fig. 8 (a), under the impact of $R_s \neq 0\Omega$, I–V curve shows exponential-like kink in the first quadrant. Obviously, it is neither exponential nor linear types.

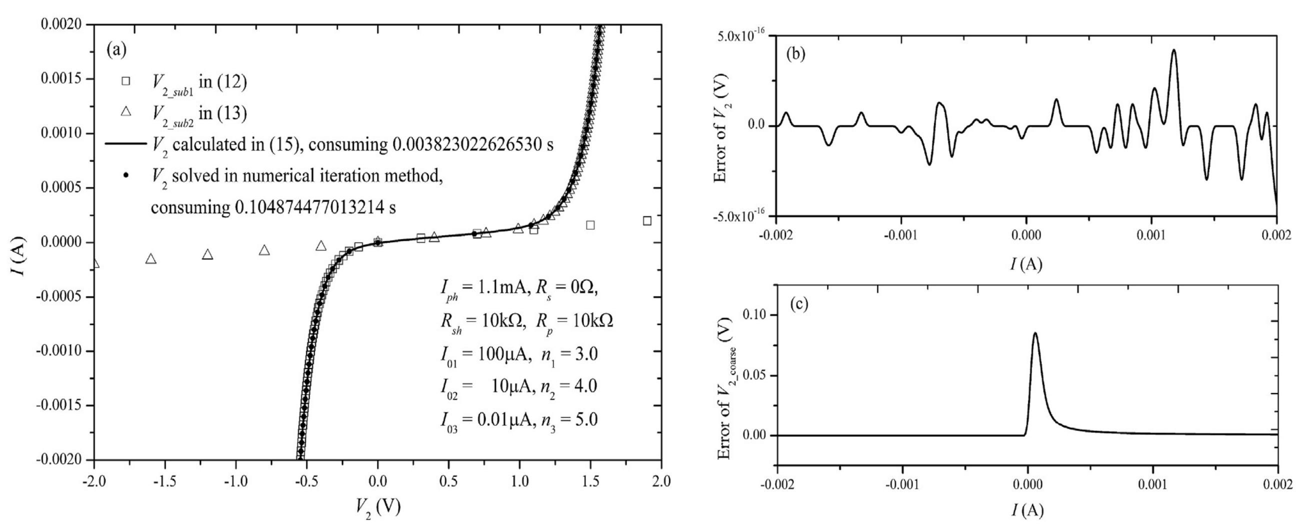

Fig. 5. (a) I vs. V_2 curves, (b) error of V_2 between the proposed analytical solution (15) and numerical iteration results, (c) error of V_2 between the proposed coarse solution V_{2_coarse} solution (14) and numerical iteration results.

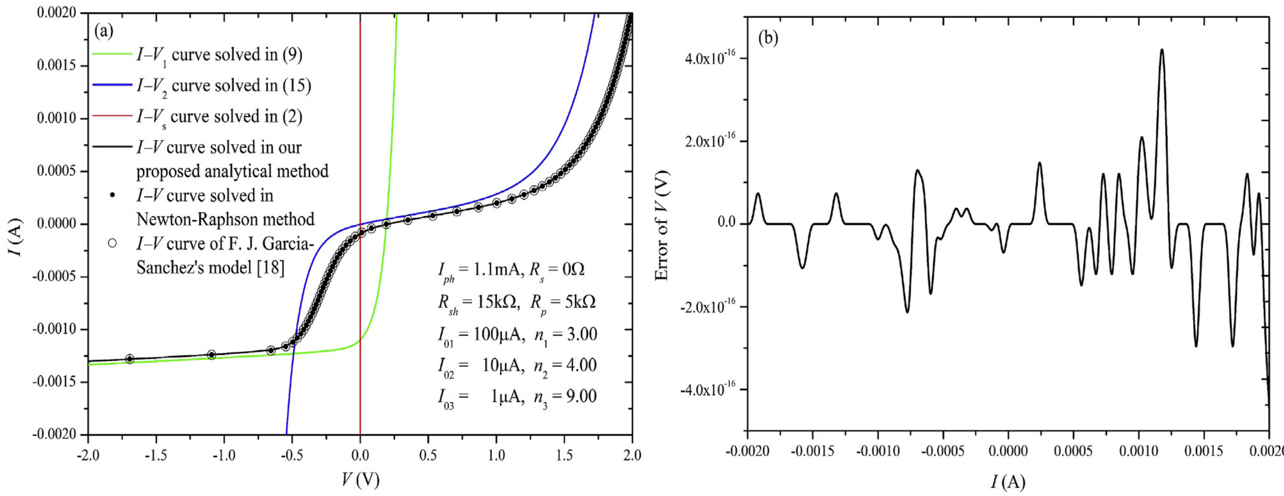

Fig. 6. (a) I vs. V curves with exponential kinks, (b) error of V between the proposed analytical solution and numerical iteration data.

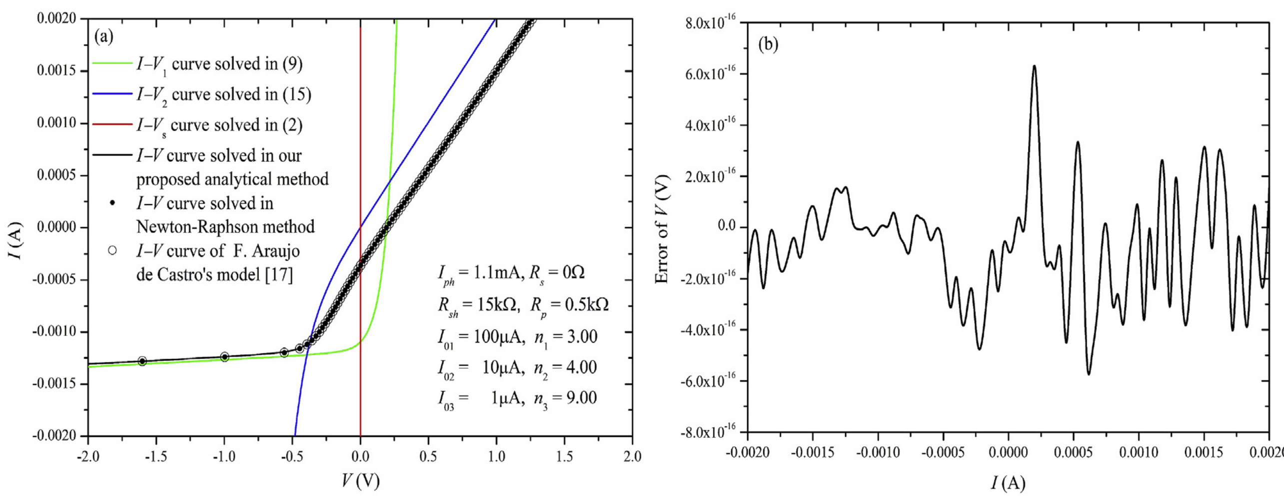

Fig. 7. (a) I vs. V curves with linear kinks, (b) error of V between the proposed analytical solution and numerical iteration data.

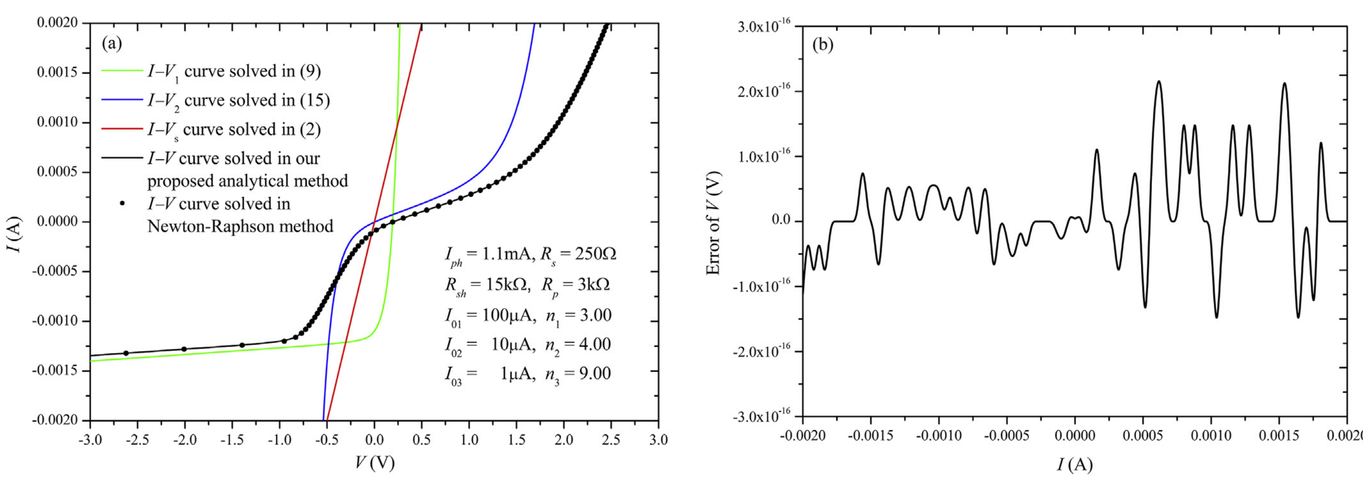

Fig. 8. (a) I vs. V curves with exponential-like kinks, (b) error of V between the proposed analytical solution and numerical iteration data.

It rises like but lower than exponent curve.

4. Experimental verifications

For the real solar cells, all of device materials, reparation processes, and operation environments are able to affect *I*–*V* characteristics. From the view point of device materials, S-shaped *I*–*V* curves are regularly observed in experiments measured from perovskite and organic solar cells [32–34]. According to Figs. 9–11, our proposed analytical solution to P. J. Roland's lumped-parameter equivalent circuit model [23] possesses enough capabilities to predict and simulate S-shaped *I*–*V* curves with linear, exponential, or exponential-like kinks. The fitting parameters used in simulations are also listed in Figs. 9–11, that can be extracted through the common routine of the parameter acquisition [35] based on

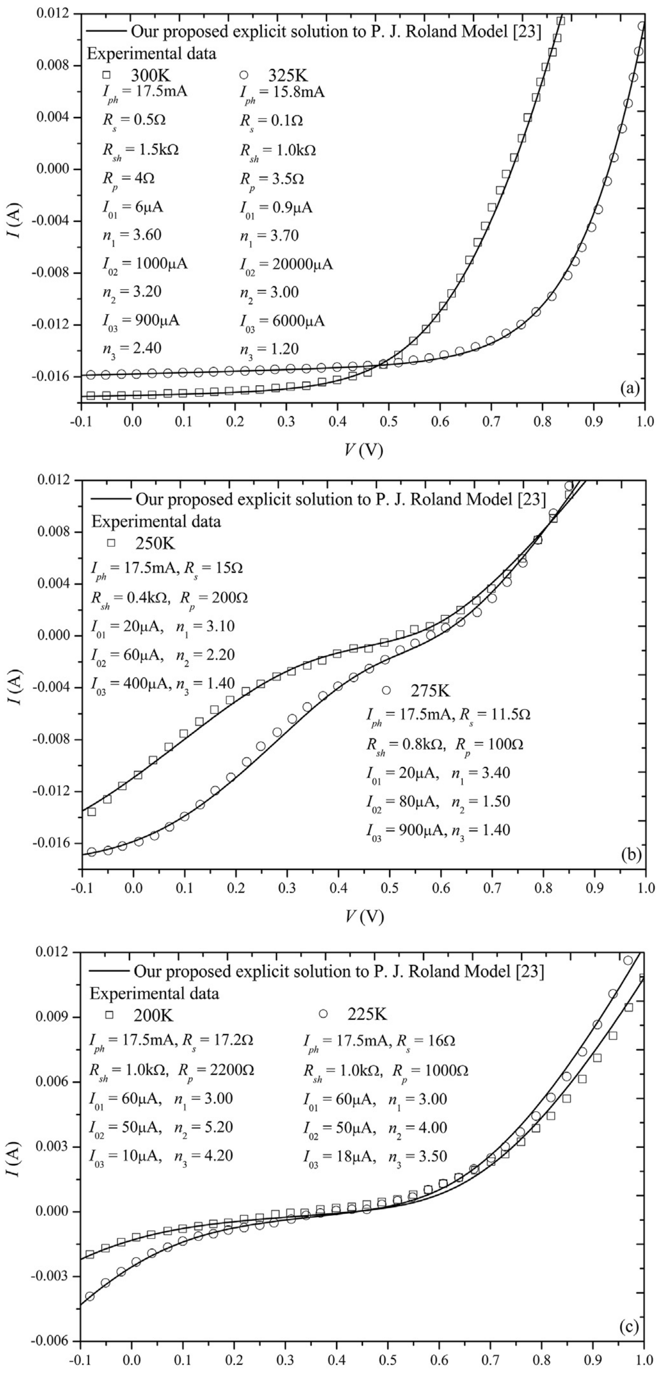

Fig. 9. Comparisons between simulation results of our explicit solution to P. J. Roland's model [23] in Fig. 1 and reconstructed experimental data [32] measured from perovskite solar cells at the different operating temperatures varied from 200 K to 325 K. (a) J-shaped *I* vs. *V* curves above room temperature (300 K and 325 K), (b) S-shaped *I* vs. *V* curves with linear kinks around room temperature (250 K and 275 K), (c) S-shaped *I* vs. *V* curves with exponential-like kinks below room temperature (200 K and 225 K).

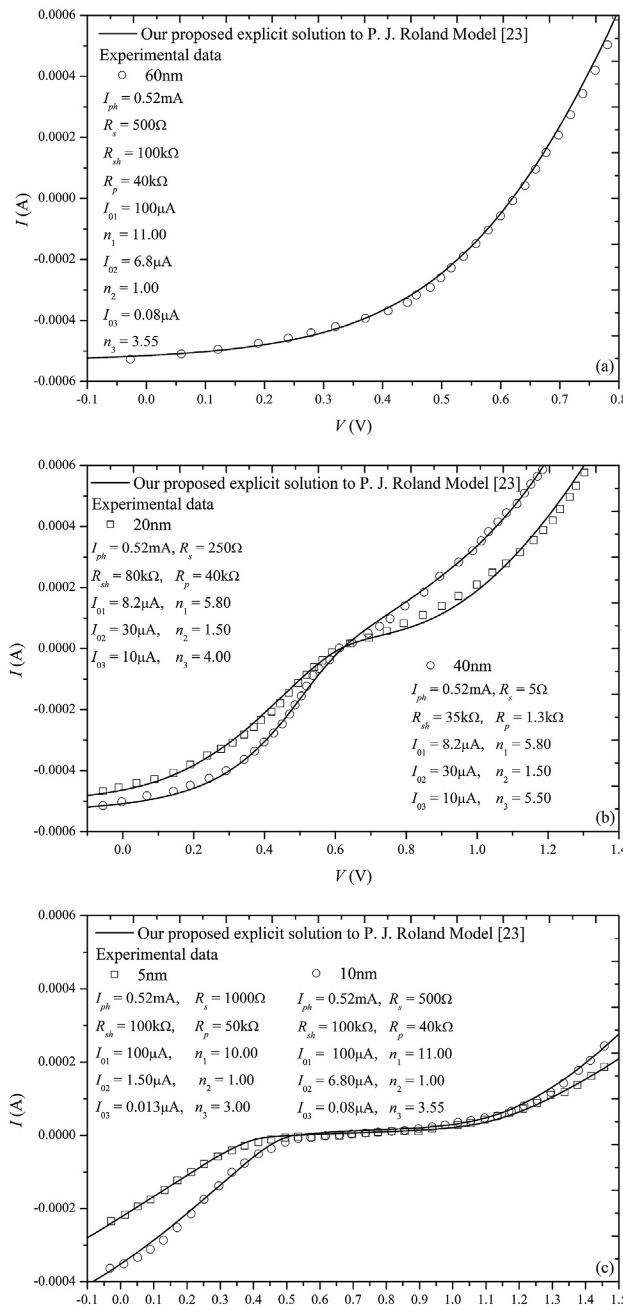

Fig. 10. Comparisons between simulation results of our analytical solution to P. J. Roland's model [23] in Fig. 1 and reconstructed experimental data [33] measured from organic solar cells with the different thicknesses of aluminum cathode varied from 5 nm to 60 nm. (a) J-shaped *I* vs. *V* curves of organic solar cells with 60 nm aluminum cathode thickness, (b) S-shaped *I* vs. *V* curves of organic solar cells with 40 nm and 20 nm aluminum cathode thicknesses, (c) S-shaped *I* vs. *V* curves of organic solar cells with 10 nm and 5 nm aluminum cathode thicknesses.

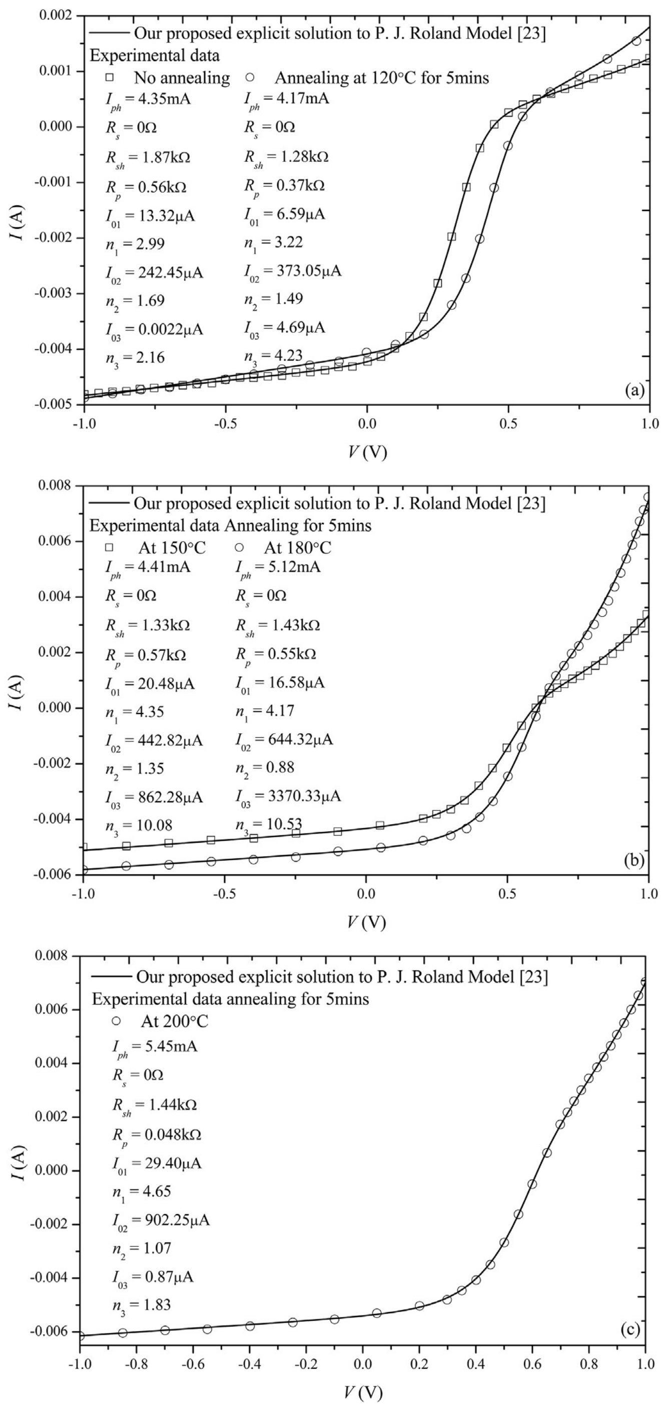

Fig. 11. Comparisons between simulation results of our analytical solution to P. J. Roland's model [23] in Fig. 1 and reconstructed experimental data [34] measured from organic solar cells annealing for 5 min at the different temperatures. (a) S-shaped *I* vs. *V* curves with linear kinks of organic solar cells with no annealing and annealing at 120 °C, (b) S-shaped *I* vs. *V* curves with exponential-like kinks of organic solar cells with annealing at 150 °C and 180 °C, (c) J-shaped *I* vs. *V* curves of organic solar cells with annealing at 200 °C.

intelligent computational algorithms.

In Fig. 9, our proposed explicit solution to P. J. Roland's model provides the accurate simulations for J- and S-shaped *I*–*V* curves of perovskite solar cells [32] measured under AM1.5G(100 mW/cm^2) illumination and at the different operating temperatures, i.e., below room temperature (200 K and 225 K), around room temperature (250 K and 275 K), above room temperature (300 K and 325 K), respectively. By using one-step solution process, the planar perovskite solar cells [32], with Au electrode deposited by thermal evaporation, were prepared on 200 nm fluorine-doped thin oxide (FTO) glass substrates. The perovskite solar cells [32] consist of 30 nm compact TiO2 layer, 300 nm perovskite absorber layer, and 500 nm hole-transporting material (HTM) layer. Firstly, above room temperature (300 K and 325 K), *I*–*V* characteristics of perovskite solar cells show J-shaped curves instead of S-shaped curves, as shown in Fig. 9(a). It is noted that the values of R_p in P. J. Roland's model are so much small that the current of R_p in Fig. 1 dominates the current of sub-circuit 2. This point shows that, based on our above analysis, P. J. Roland's model actually could degrade into the conventional single-diode model in Fig. 2 for describing the J-shaped curve. Secondly, around room temperature (250 K and 275 K), *I*–*V* characteristics of perovskite solar cells show S-shaped curves with linear kinks, as shown in Fig. 9(b). In this case, our proposed explicit solution to P. J. Roland's model still gives accurate descriptions about linear kinks with the help of medium R_p. In other words, this point is consistent with (6) so that P. J. Roland's model could transform into the F. Araujo de Castro's model in Fig. 4 for describing the S-shaped curves with linear kinks. Thirdly, below room temperature (200 K and 225 K), *I*–*V* characteristics of perovskite solar cells show S-shaped curves with exponential-like kinks, as shown in Fig. 9(c). On this condition, our proposed explicit solution to P. J. Roland's model still gives accurate descriptions about exponential-like kinks with the help of large R_p. In fact, this point is also consistent with (8) so that P. J. Roland's model could predict the S-shaped curves with exponential-like kinks.

In Fig. 10, in the cases of different cathode thicknesses, our proposed explicit solution to P. J. Roland's model has still an ability of accurately predicting the J- and S-shaped *I*–*V* curves of organic solar cells. In the preparation processes of the ITO/PEDOT-PSS/P3HT:PCBM/Al organic solar cells [33], PEDOT-PSS coated on indium tin oxide (ITO) substrates was placed on a hotplate and dried, P3HT:PCBM solution was then deposited on PEDOT:PSS covered ITO substrate, and then aluminum was deposited as electrodes with layer thickness of 5 nm, 10 nm, 20 nm, 40 nm, 60 nm. For the enough thickness of aluminum cathode, locating in the range [60 nm, ∞), J-shaped *I*–*V* curves are predicted by our proposed explicit solution to P. J. Roland's model, as shown in Fig. 10(a); For the medium thickness of aluminum cathode, locating in the range [20 nm, 40 nm], S-shaped *I*–*V* curves with exponential-like kinks could be simulated by our proposed explicit solution to P. J. Roland's model, as shown in Fig. 10(b); For the small thickness of aluminum cathode, locating in the range (0 nm, 20 nm], S-shaped *I*–*V* curves with exponential-like kinks are also described accurately by our proposed explicit solution to P. J. Roland's model, as shown in Fig. 10(c). According to Fig. 10 (b) and (c), exponential characteristics dominate exponential-like kinks for relative large electrode layer thickness, while linear characteristics dominate exponential-like kinks for relative small electrode layer thickness. In fact, both R_p and D_3 determine the shapes of the kink curves in *I*–*V* characteristics of organic solar cells.

In Fig. 11, for the different annealing temperatures, our proposed explicit solution to P. J. Roland's model actually describes the J- and S-shaped *I*–*V* curves of organic solar cells [34] with the different annealing temperatures. In Fig. 11(a), for the cases of no annealing and annealing at low temperatures (<150 °C), linear kinks in the first quadrant are obviously observed in the S-shaped *I*–*V* curves of organic solar cells [34]. In Fig. 11(b), for the cases of annealing at medium temperatures (larger than 150 °C and lower than 180 °C), exponential-like kinks in the first quadrant are observed in the S-shaped *I*–*V* curves of organic solar cells [34]. In Fig. 11(c), J-shaped *I*–*V* curve is also observed in organic solar cells [34] for the cases of annealing at high temperatures (>200 °C).

5. Conclusions

In this paper, an explicit solution to P. J. Roland's lumped-parameter equivalent circuit model is proposed to accurately and efficiently simulate new generation solar cells' both J-shaped *I*−*V* characteristics and S-shaped *I*−*V* characteristics with linear, exponential, or exponential-like current kinks. Based on the regional approach, terminal voltages of P. J. Roland's model are analytically solved and then corrected to avoid the use of numerical iteration algorithms. Furthermore, numerical iteration algorithms are adopted to solve complicated transcend equations including three exponential items and numerical iteration results are used to verify the accuracy of our proposed explicit solution to P. J. Roland's model. Finally, reconstructed experimental results measured from perovskite and organic solar cells are also used to verify the applicability of our proposed explicit solution. In fact, such an explicit solution could be used to extend the application range of P. J. Roland's model, complete analysis for S-shaped *I*−*V* characteristics of new generation solar cells, and facilitate researchers implement P. J. Roland's model into solar cells' simulations.

Declaration of competing interest

The authors declare that they have no known competing financial interests or personal relationships that could have appeared to influence the work reported in this paper.

Acknowledgment

This work was supported in part by the National Natural Science Foundation of China under grant 61904056 and in part by the Fundamental Research Funds for the Central Universities under Grant ZQN-809.

References

[1] Petti L, Munzenrieder N, Vogt C, Faber H, Buthe L, Cantarella G, Bottacchi F, Anthopoulos TD, Troster G. Metal oxide semiconductor thin-film transistors for flexible electronics. Appl Phys Rev Jun. 2016;3(2):021303.
[2] Arora N, Dar MI, Hinderhofer A, Pellet N, Schreiber F, Zakeeruddin SM, Gratzel M. Perovskite solar cells with CuSCN hole extraction layers yield stabilized efficiencies greater than 20%. Science Nov. 2017;358(6364):768−71.
[3] Jodlowski AD, Roldan-Carmona C, Grancini G, Salado M, Ralaiarisoa M, Ahmad S, Koch N, Camacho L, de Miguel D, Nazeeruddin MK. Large guanidinium cation mixed with methylammonium in lead iodide perovskites for 19% efficient solar cells. Nat Energy Dec. 2017;2(12):972−9.
[4] Jiang Q, Chu Z, Wang P, Yang X, Liu H, Wang Y, Yin Z, Wu J, Zhang X, You J. Planar-Structure perovskite solar cells with efficiency beyond 21%. Adv Mater Dec. 2017;29(46):1703852.
[5] Sahli F, Werner J, Kamino BA, Brauninger M, Monnard R, Paviet-Salomon B, Barraud L, Ding L, Leon JJD, Sacchetto D, Cattaneo G, Despeisse M, Boccard M, Nicolay S, Jeangros Q, Niesen B, Ballif C. Fully textured monolithic perovskite/silicon tandem solar cells with 25.2% power conversion efficiency. Nat Mater Sep. 2018;17(9):820.
[6] Park S, Heo SW, Lee W, Inoue D, Jiang Z, Yu K, Jinno H, Hashizume D, Sekino M, Yokota T, Fukuda K, Tajima K, Someya T. Self-powered ultra-flexible electronics via nano-grating-patterned organic photovoltaics. Nature Sep. 2018;561(7724):516.
[7] Meng L, Zhang Y, Wan X, Li C, Zhang X, Wang Y, Ke X, Xiao Z, Ding L, Xia R, Yip HL, Cao Y, Chen Y. Organic and solution-processed tandem solar cells with 17.3% efficiency. Science Sep. 2018;361(6407):1094.
[8] Zhou Z, Xu S, Song J, Jin Y, Yue Q, Qian Y, Liu F, Zhang F, Zhu X. High-efficiency small-molecule ternary solar cells with a hierarchical morphology enabled by synergizing fullerene and non-fullerene acceptors. Nat Energy Nov. 2018;3(11):952−9.
[9] Wadsworth A, Moser M, Marks A, Little MS, Gasparini N, Brabec CJ, Baran D, McCulloch I. Critical review of the molecular design progress in non-fullerene electron acceptors towards commercially viable organic solar cells. Chem Soc Rev Mar. 2019;48(6):1596−625.
[10] Yoshikawa K, Kawasaki H, Yoshida W, Irie T, Konishi K, Nakano K, Uto T, Adachi D, Kanematsu M, Uzu H, Yamamoto K. Silicon heterojunction solar cell with interdigitated back contacts for a photoconversion efficiency over 26%. Nat Energy May. 2017;2(5):17032.
[11] Garcia-Sanchez FJ, Romero B, Lugo-Munoz DC, Del Pozo G, Arredondo B, Liou JJ, Ortiz-Conde A. "Modelling solar cell S-shaped I-V characteristics with DC lumped-parameter equivalent circuits − a review. Facta Univ − Ser Electron Energetics Sep. 2017;30(3):327−50.
[12] Khatibi A, Astaraei FR, Ahmadi MH. Generation and combination of the solar cells: a current model review. Energy Sci Eng Apr. 2019;7(2):305−22.
[13] Li D, Song L, Chen Y, Huang W. Modeling thin film solar cells: from organic to perovskite. Adv Sci Nov. 2019:1901397.
[14] Jain A, Kapoor A. Exact analytical solutions of the parameters of real solar cells using Lambert W-function. Sol Energy Mater Sol Cells Feb. 2004;81(2):269−77.
[15] Jain A, Kapoor A. A new approach to study organic solar cell using Lambert W-function. Sol Energy Mater Sol Cells Mar. 2005;86(2):197−205.
[16] Ortiz-Conde A, Lugo-Muñoz D, García Sánchez FJ. An explicit multi-exponential model as an alternative to traditional solar cell models with series and shunt resistances. IEEE J Photovolt Jul. 2012;2(3):261−8.
[17] Araujo de Castro F, Heier J, Nüesch F, Hany R. Origin of the kink in current-density versus voltage curves and efficiency enhancement of polymer-C60 heterojunction solar cells. IEEE J Sel Top Quant Electron Nov/Dec. 2010;16(6):1690−9.
[18] García-Sánchez FJ, Lugo-Muñoz D, Muci J, Ortiz-Conde A. "Lumped parameter modeling of organic solar cells' S-shaped I-V characteristics. IEEE J Photovolt Jan. 2013;3(1):330−5.
[19] Mazhari B. An improved solar cell circuit model for organic solar cells. Sol Energy Mater Sol Cells May. 2006;90(7):1021−33.
[20] Romero B, del Pozo G, Arredondo B, Martín-Martín D, Ruiz Gordoa MP, Pickering A, Pérez-Rodríguez A, Barrena E, García-Sánchez FJ, "S-Shaped IV. Characteristics of organic solar cells: solving mazhari's lumped-parameter equivalent circuit model. IEEE Trans Electron Dev Nov. 2017;64(11):4622−7.
[21] Yu F, Huang G, Lin W, Xu C. An analysis for S-shaped I-V characteristics of organic solar cells using lumped-parameter equivalent circuit model. Sol Energy Jan. 2019;177(1):229−40.
[22] Yu F, Huang G, Lin W, Xu C. "Lumped-Parameter equivalent circuit model for S-shaped current−voltage characteristics of organic solar cells. IEEE Trans Electron Dev Jan. 2019;66(1):670−7.
[23] Roland PJ, Bhandari KP, Ellingson RJ. Electronic circuit model for evaluating S-kink distorted current-voltage curves. In: Proc. IEEE 43rd photovoltaic specialists conf. (PVSC); 2016.
[24] Yu F, Huang G, Xu C. An explicit method to extract fitting parameters in lumped-parameter equivalent circuit model of industrial solar cells. Renew Energy Feb. 2020;146:2188−98.
[25] Shockley W. The theory of p-n junctions in semiconductors and p-n junction transistors. Bell Syst Tech J Jul. 1949;28(3):435−89.
[26] Corless RM, Gonnet GH, Hare DEG, Jeffrey DJ, Knuth DE. "On Lambert's W function. Adv Comput Math May. 1996;5(1):329−59.
[27] Yu F, Deng W, Huang J, Ma X, Chen S. An explicit physics-based I-V model for surrounding-gate polysilicon transistors. IEEE Trans Electron Dev Mar. 2016;63(3):1059−65.
[28] Yu F, Ma X, Deng W, Liou JJ, Huang J. A surface-potential-based drain current compact model for a-InGaZnO thin-film transistors in Non-Degenerate conduction regime. Solid State Electron Nov. 2017;137(11):38−43.
[29] Fang J, Deng W, Ma X, Huang J, Wu W. A surface-potential-based DC model of amorphous oxide semiconductor TFTs including degeneration. IEEE Electron Device Lett Feb. 2017;38(2):183−6.
[30] Ghittorelli M, Torricelli F, Kovacs-Vajna ZM. Analytical physical-based drain-current model of amorphous InGaZnO TFTs accounting for both non-degenerate and degenerate conduction. IEEE Electron Device Lett Dec. 2015;36(12):1340−3.
[31] Chen R, Zheng X, Deng W, Wu Z. A physics-based analytical solution to the surface potential of polysilicon thin film transistors using the lambert *W* function. Solid State Electron Jun. 2007;51(6):975−81.
[32] Xu F, Zhu J, Cao R, Ge S, Wang W, Xu H, Xu R, Wu Y, Gao M, Ma Z, Jiang Z. Elucidating the evolution of the current-voltage characteristics of planar organometal halide perovskite solar cells to an S-shape at low temperature. Sol Energy Mater Sol Cells Aug. 2016;157:981−8.
[33] Sesa E, Darwis D, Zhou X, Belcher WJ, Dastoor PC. "Experimental determination of the relationship between the elements of a back-to-back diode model for organic photovoltaic cells' S-shaped *I-V* characteristics and cell structure. AIP Adv Feb. 2019;9(2):025014.
[34] De Castro F, Laudani A, Fulginei FR, Salvini A. An in-depth analysis of the modelling of organic solar cells using multiple-diode circuits. Sol Energy Oct. 2016;135:590−7.
[35] Wei T, Yu F, Huang G, Xu C. A particle-swarm-optimization-based parameter extraction routine for three-diode lumped parameter model of organic solar cells. IEEE Electron Device Lett Sep. 2019;40(9):1511−4.